International Scholarly Research Network
ISRN Renewable Energy
Volume 2011, Article ID 634025, 13 pages
doi:10.5402/2011/634025

Research Article

Performance Study of Solar Air Heater Having Absorber Plate with Half-Perforated Baffles

B. K. Maheshwari, Rajendra Karwa, and S. K. Gharai

Department of Mechanical Engineering, Faculty of Engineering and Architecture, J.N. Vyas University, Jodhpur 342011, India

Correspondence should be addressed to Rajendra Karwa, karwa_r@yahoo.com

Received 4 July 2011; Accepted 11 August 2011

Academic Editors: C. Cristofari and B. Mwinyiwiwa

The paper presents a detailed mathematical model for performance prediction of a smooth duct solar air heater validated against the experimental results. Experimental study on a solar air heater having absorber plate with half-perforated baffles on the air flow side shows thermal efficiency enhancement of 28%–45% over that of the smooth duct solar air heater, which is attributed to the heat transfer enhancement (of the order of 180%–235%) due to the perforated baffles attached to the absorber plate and reduction in the mean temperature of the absorber plate by 20°C–25°C as compared to the temperature of absorber plate of smooth duct air heater. Using the mathematical model, the performance plot for the baffled duct air heater has been presented, and the effect of the variation of ambient parameters on the predicted thermal efficiency has been studied.

1. Introduction

Flat plate collectors have been used to deliver heated air for space heating, crop drying, and similar applications requiring air at low-to-medium temperature (slightly above the ambient to about 100°C). The thermal efficiency of a smooth duct flat plate solar air hater is lower than that of a solar water heater because of a low value of heat transfer coefficient between the absorber plate and the air flowing through the collector duct. This leads to a high operating temperature of the collector, especially the absorber plate, resulting in greater heat loss from the collector. Hence, the researchers have directed their efforts towards enhancement of heat transfer coefficient by creating turbulence near the heat transferring surface using artificial roughness in various forms, such as solid roughness elements of various shapes and in different arrangements and perforated or detached roughness elements [1–18].

The solid roughness elements have been shown to significantly enhance the heat transfer coefficient, but the associated increase in the friction factor is of serious concern. Further, hot zones develop in the wake of these roughness elements because of a recirculating flow in the wake region. The detached elements or elements with perforations allow a part of the flow to pass through the perforations or gap, and thus, the adverse effects of the hot zone and form drag are reduced [12–18]. Hwang and Liou in [14] studied the effect of the half-perforated turbulence promoters symmetrically mounted on two opposite walls on the heat transfer and friction in a rectangular channel. They found that the half-perforated turbulence promoters with perforations on the lower half of the ribs performed better than those with the solid type or fully perforated promoters.

In the transitional flow regime (Re $\leq$ 10000), which is of interest in the solar air heaters, the resistance to the heat transfer extends up to the buffer layer between the laminar sublayer and turbulent core. Hence, elements projecting beyond the sublayer, such as baffles, may be useful. To enhance the heat transfer in an asymmetrically heated rectangular section duct, Karwa et al. [17] employed solid and fully perforated baffles attached to the uniformly heated broad wall of the duct. Karwa and Maheshwari [18] carried out an experimental study of heat transfer and friction in such ducts with fully perforated (open area ratio of 46.8%) or half-perforated baffles (open area ratio of 26%) at pitch to baffle height ratio of 7.2–28.8 and flow

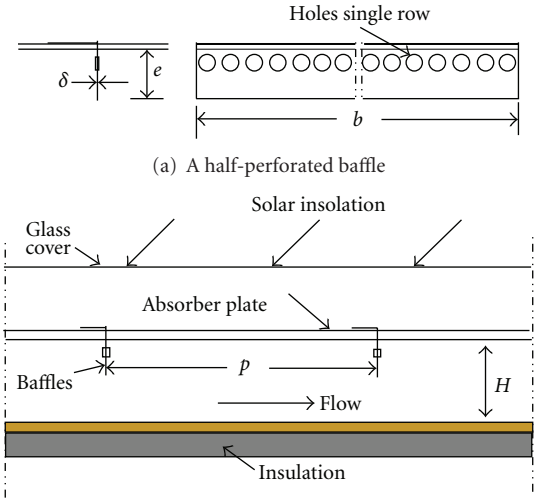

(a) A half-perforated baffle

(b) Longitudinal section of the solar air heater

Figure 1: Solar air heater with perforated baffles.

Reynolds number of 2700 to 11150. The study showed an enhancement of 79%–169% and 133%–274% in the Nusselt number over the smooth duct for the fully perforated and half-perforated baffles, respectively, while the friction factor values are reported to be 2.98–8.02 and 4.42–17.5 times of that for the smooth duct, respectively. They found that the half-perforated baffles at a pitch to baffle height ratio of 7.2 provided the greatest performance advantage of 51%–75% over a smooth duct at equal pumping power.

Since the boundary conditions in the studies of Karwa and coauthors [17, 18] correspond closely to those found in solar air heaters, the objective of the present experimental study has been to study the effectiveness of the half-perforated baffles in the solar air heater duct in the thermal performance enhancement. Half-perforated baffles of Karwa and Maheshwari [18], as shown in Figure 1, have been used with the absorber plate of the baffled duct air heater. A mathematical model for the performance prediction of the smooth duct solar air heater is also to be presented and validated against the experimental results for such air heater so that the same can be used for the performance prediction of smooth or baffled duct air heaters under a range of operating conditions.

2. Mathematical Model for Performance Prediction

Karwa and Chauhan [19] have presented a detailed nonlinear mathematical model for a smooth duct solar air heater. The model calculates the useful heat gain from the iterative solution of basic heat transfer equations of top loss and equates the same with the convective heat transfer from the absorber plate to the air using proper heat transfer correlations for the smooth duct air heater. The back loss from the collector is calculated from the iterative solution of the heat balance equation for the back surface, while the edge loss is estimated from the equation suggested by Klein [20].

Figure 2 shows the schematic diagram of a solar air heater. The heat balance on the air heater gives the distribution of incident solar radiation I into useful heat gain Q and the heat loss Q_L. The useful heat gain or heat collection rate can be expressed as

$$Q = AI\,(\tau\alpha) - Q_L = A\left[I\,(\tau\alpha) - U_L\left(T_p - T_a\right)\right], \quad (1)$$

where A is the area of the absorber plate, $(\tau\alpha)$ is the transmittance-absorptance product of the glass cover-absorber plate combination. The heat loss Q_L from the collector is a sum of the losses from top Q_t, back Q_b and edge Q_e of the collector as depicted in Figure 2.

The factor U_L in (1) is termed as overall loss coefficient and is defined as

$$U_L = \frac{Q_L}{\left[A\left(T_p - T_a\right)\right]}, \quad (2)$$

where T_p is the mean absorber plate temperature and T_a is the ambient temperature.

The collected heat is transferred to the air flowing through the air heater duct. Thus,

$$Q = mc_p(T_o - T_i) = GAc_p(T_o - T_i), \quad (3)$$

where m is the air flow rate through the collector duct and $G(= m/A)$ is flow rate of air per unit area of the absorber plate.

From the heat transfer consideration, the heat gain is

$$Q = hA\left(T_p - T_m\right), \quad (4)$$

where T_m is the mean temperature of air in the solar air heater duct and h is the heat transfer coefficient.

2.1. Top Loss. The heat loss from the collector glass cover, termed as top loss Q_t, is calculated from the iterative solution of the basic heat transfer equations given below.

Heat transfer from absorber plate at a mean temperature T_p to the inner surface of the glass at temperature T_{gi} takes place by radiation and convection. Hence,

$$Q_{tpg} = A\left[\sigma\left(T_p^4 - T_{gi}^4\right)\left(\frac{1}{\varepsilon_p} + \frac{1}{\varepsilon_g} - 1\right)^{-1} + h_{pg}\left(T_p - T_{gi}\right)\right], \quad (5)$$

where ε_p and ε_g are the emissivity of the absorber plate and the glass cover, respectively, and h_{pg} is the convection heat transfer coefficient.

The conduction heat transfer through the glass cover of thickness δ_g is given by

$$Q_{tg} = \frac{k_g A\left(T_{gi} - T_{go}\right)}{\delta_g}, \quad (6)$$

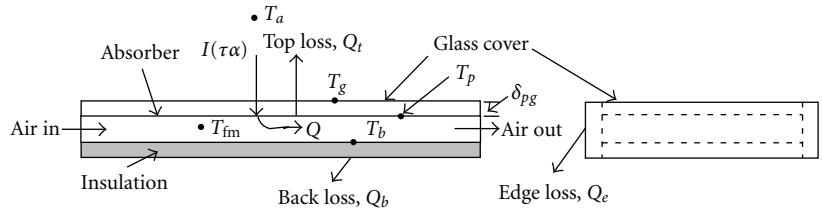

Figure 2: Heat balance on a solar air heater.

where k_g is the thermal conductivity of the glass and T_{go} is temperature of the outer surface of the glass.

From the outer surface of the glass cover, the heat is rejected by radiation to the sky at temperature T_s and by convection to the ambient. Hence,

$$Q_{tgo} = A\left[\sigma\varepsilon_g\left(T_{go}^4 - T_s^4\right) + h_w\left(T_{go} - T_a\right)\right], \tag{7}$$

where h_w is termed as wind heat transfer coefficient. It can be considered to be about 5–10 $\text{Wm}^{-2}\text{K}^{-1}$ (corresponding to the no wind to the usually encountered maximum wind velocity in the western part of Rajasthan, India). The sky temperature T_s is a function of many parameters. Some studies assume the sky temperature to be equal to the ambient temperature, because it is difficult to make a correct estimate of it, while others estimate it using different correlations.

In the equilibrium,

$$Q_{tpg} = Q_{tg} = Q_{tgo} = Q_t. \tag{8}$$

To estimate of the convective heat transfer coefficient between the absorber plate and glass cover h_{pg}, the following three-region correlation of Buchberg et al. [21] has been used:

$$\text{Nu} = 1 + 1.446\left(1 - \frac{1708}{\text{Ra}'}\right)^{+} \quad \text{for } 1708 \le \text{Ra}' \le 5900$$

$$(+ \text{ bracket goes to zero when negative}), \tag{9a}$$

$$\text{Nu} = 0.229(\text{Ra}')^{0.252} \quad \text{for } 5900 < \text{Ra}' \le 9.23 \times 10^4, \tag{9b}$$

$$\text{Nu} = 0.157(\text{Ra}')^{0.285} \quad \text{for } 9.23 \times 10^4 < \text{Ra}' \le 10^6, \tag{9c}$$

where $\text{Ra}'(= \text{Ra}\cos\beta)$ is Rayleigh number for the inclined air layers between the absorber plate and glass cover (collector slope $\beta = 0^\circ$ for horizontal). The Rayleigh number is given by

$$\text{Ra} = \text{Gr}\,\text{Pr} = \left[g\left(T_p - T_{gi}\right)\frac{{\delta_{pg}}^3}{\left(T_{mpg}\nu_{mpg}^2\right)}\right]\text{Pr}, \tag{10}$$

where δ_{pg} = gap between the absorber plate and glass cover, T_{mpg} is the mean temperature of the air in the gap, and ν_{mpg} is the kinematic viscosity of the air at T_{mpg}.

2.2. Back and Edge Losses. The back loss from the collector, refer to Figure 2, is calculated from the following equation

$$Q_b = \frac{A(T_b - T_a)}{(\delta/k_i + 1/h_w)}, \tag{11a}$$

where δ is the insulation thickness, k_i is the thermal conductivity of the insulating material and T_b is the temperature of the bottom surface of the collector duct, which has been estimated from the iterative solution of the heat balance equation detailed below.

Heat transfer by radiation from the heated absorber plate to the duct bottom surface Q_{pb} is calculated from

$$Q_{pb} = \sigma\left(T_p^4 - T_b^4\right)\left(\frac{1}{\varepsilon_{pi}} + \frac{1}{\varepsilon_b} - 1\right)^{-1}. \tag{11b}$$

The heat flows from the heated bottom surface to the surroundings through the back insulation and to the air flowing through the duct at mean temperature T_m; that is,

$$Q_{ba} = \frac{(T_b - T_a)}{(\delta/k_i + 1/h_w)} + h(T_b - T_m). \tag{11c}$$

The absorber plate inner surface and duct bottom surface long wave emissivity values ε_{pi} and ε_b in (11b) have been assumed to be 0.9. The heat balance for the surface gives $Q_{pb} = Q_{ba}$.

For the estimate of the edge loss, the empirical equation suggested by Klein [20] has been used, which is

$$Q_e = 0.5A_e\left(T_p - T_a\right), \tag{12}$$

where A_e is the area of the edge of the air heater rejecting heat to the surroundings.

Knowing the useful heat gain Q, the outlet air temperature is calculated from

$$T_o = T_i + \frac{Q}{\left(mc_p\right)}. \tag{13}$$

The thermal efficiency η of the solar air heater is the ratio of the useful heat gain Q and the incident solar radiation I on the collector plane; that is,

$$\eta = \frac{Q}{(IA)}. \tag{14}$$

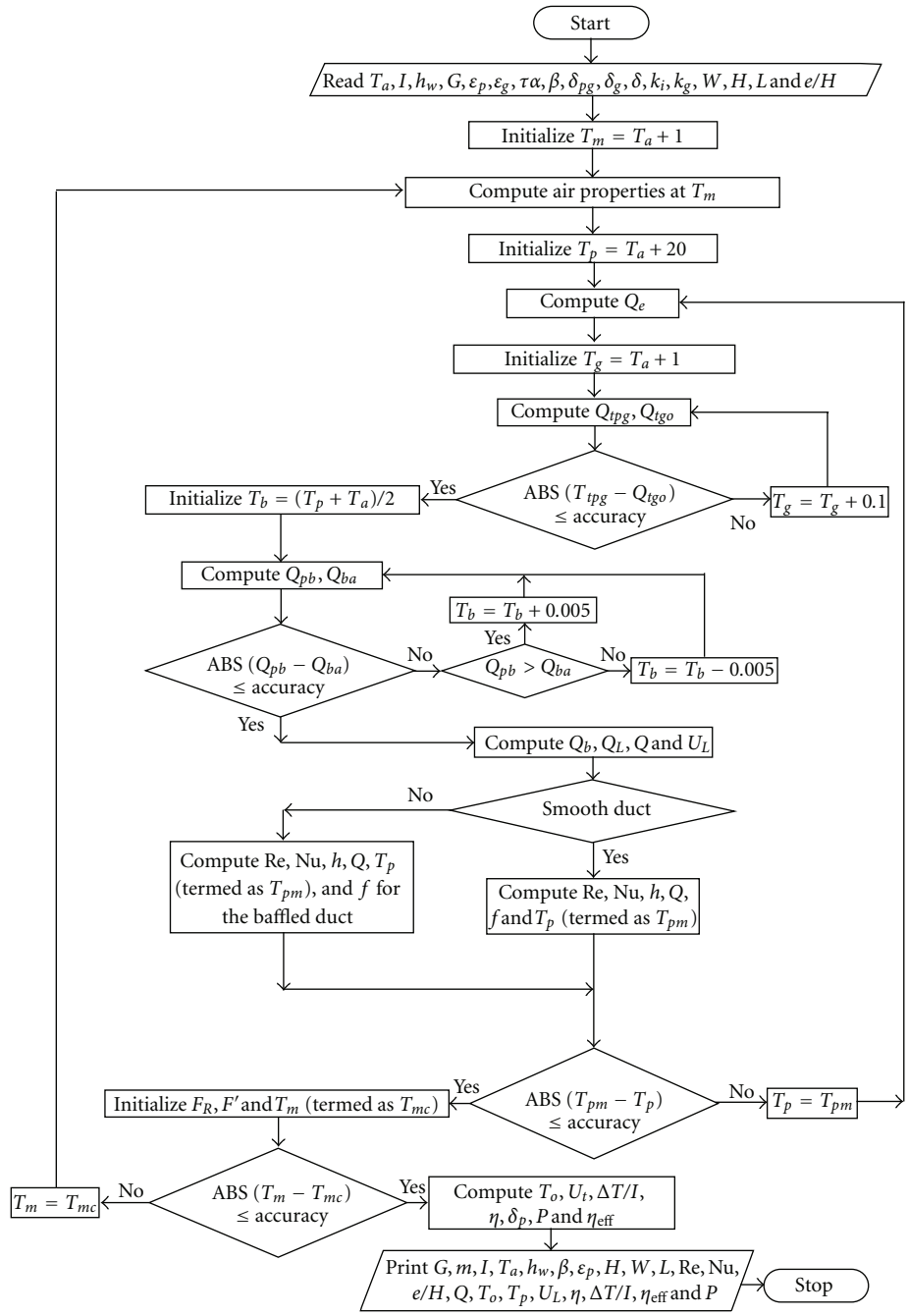

Figure 3: Flow chart for iterative solution of mathematical model.

Niles et al. [22] used the following equations to calculate the outlet air and mean plate temperatures when the solar air heater operates in open loop mode (i.e., $T_i = T_a$):

$$T_o = T_a + \frac{I(\tau\alpha)\xi}{U_L}, \tag{15a}$$

$$T_p = T_i + \left[\frac{I(\tau\alpha)}{U_L}\right]\left(1 - G\xi\frac{c_p}{U_L}\right), \tag{15b}$$

where $\xi = 1 - \exp[-U_L/(Gc_p)(1 + U_L/h)^{-1}] = (F_R\ U_L/Gc_p)$. Parameter F_R is termed as heat removal factor and is given by

$$F_R = \left(\frac{Gc_p}{U_L}\right)\left[1 - \exp\left(-F'\frac{U_L}{Gc_p}\right)\right], \tag{16}$$

where F' is termed as efficiency factor. It is given by

$$F' = \left(1 + \frac{U_L}{h}\right)^{-1}. \tag{17}$$

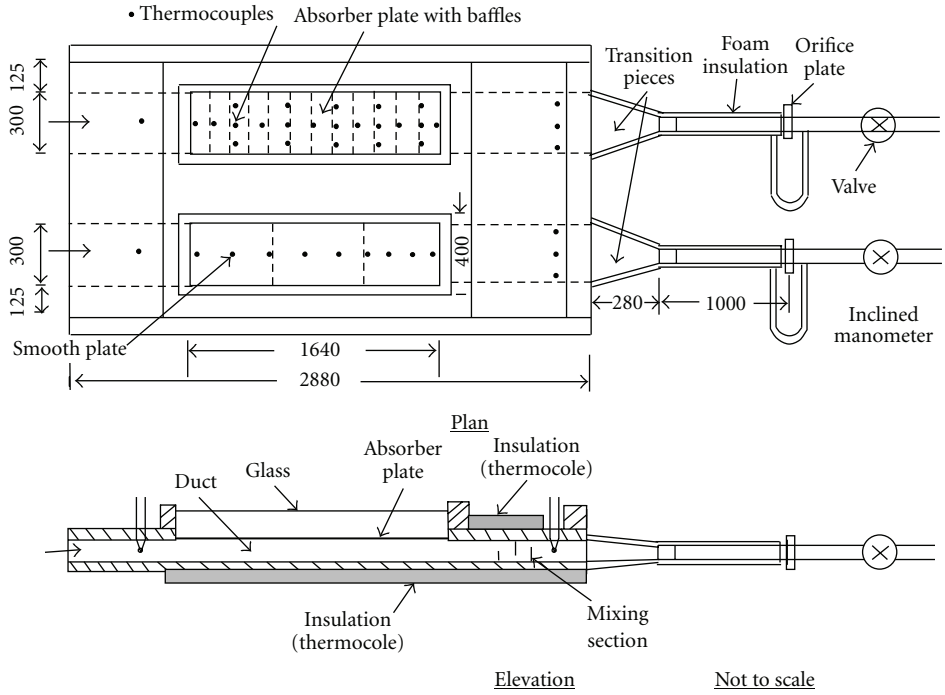

Figure 4: Experimental setup.

The mean air temperature equation in terms of heat removal factor F_R and efficiency factor F' is

$$T_m = T_i + \left[\frac{Q}{(AU_LF_R)}\right] \times \left(1 - \frac{F_R}{F'}\right). \tag{18}$$

The accuracy of the results of the performance analysis strongly depends on the use of appropriate heat transfer and friction factor correlations for the solar air heater ducts.

For the asymmetrically heated high aspect ratio rectangular ducts of smooth duct solar air heater, Karwa et al. [8] used the following correlation of Ebadian and Dong [23, Equations (5.206) and (5.207)] for the apparent friction factor in the laminar regime, which takes account of the increased friction in the entrance region of the duct

$$f_{\text{app}} = \frac{24}{\text{Re}} + \frac{(0.64\ + (38/\text{R}_e))D_h}{(4L)}. \tag{19}$$

The heat transfer correlation from Hollands and Shewen [24] for the thermally developing laminar flow for the smooth duct is

$$\text{Nu} = 5.385 + 0.148\,\text{Re}\left(\frac{H}{L}\right) \quad \text{for Re} < 2550. \tag{20}$$

The friction factor correlation of Bhatti and Shah [25] for the transition to turbulent flow regime in rectangular cross-section smooth duct ($0 \le H/W \le 1$) is

$$f = \left(1.0875\ - 0.1125\frac{H}{W}\right) f_o, \tag{21}$$

where

$$f_o = 0.0054 + 2.3 \times 10^{-8}\text{Re}^{1.5} \quad \text{for } 2100 \le \text{Re} \le 3550,$$
$$f_o = 1.28 \times 10^{-3} + 0.1143\ \text{Re}^{-0.311} \quad \text{for } 3550 < \text{Re} \le 10^7. \tag{22}$$

They report an uncertainty of ±5% in the predicted friction factors from the above correlation.

Considering the entrance region effect, the apparent friction factor in the turbulent flow regime is determined from the following relation for flat parallel plate duct [25]:

$$f_{\text{app}} = f + 0.0175\left(\frac{D_h}{L}\right). \tag{23}$$

The Nusselt number correlations for the transition and turbulent flow regimes in the rectangular solar air heater duct from Hollands and Shewen [24] are

$$\text{Nu} = 4.4 \times 10^{-4}\text{Re}^{1.2} + 9.37\text{Re}^{0.471}\left(\frac{H}{L}\right) \quad \text{for } 2550 \le \text{Re} \le 10^4 \text{ (transition flow)} \tag{24a}$$

$$\text{Nu} = 0.03\text{Re}^{0.74} + 0.788\ \text{Re}^{0.74}\left(\frac{H}{L}\right) \quad \text{for } 10^4 < \text{Re} \le 10^5 \text{ (early turbulent flow).} \tag{24b}$$

An uncertainty of an order of 5%-6% in the predicted Nusselt number can be expected [8]. As suggested by Karwa et al. [8], the laminar regime has been assumed up to Re = 2800.

The pressure loss and pumping power are calculated from

$$\delta p = \left[\frac{\left(4 f_{\text{app}}\, L\right)}{2\rho D_h}\right]\left(\frac{m}{WH}\right)^2$$
$$P = \left(\frac{m}{\rho}\right)\delta p. \tag{25}$$

The thermophysical properties of the air have been taken at the corresponding mean temperature T_m or T_{mpg} from the following relations of thermophysical properties, obtained by correlating data from NBS (U.S.) [26]:

$$c_p = 1006\left(\frac{T_m}{293}\right)^{0.0155},$$
$$k = 0.0257\left(\frac{T_m}{293}\right)^{0.86},$$
$$\mu = 1.81 \times 10^{-5}\left(\frac{T_m}{293}\right)^{0.735}, \tag{26}$$
$$\rho = 1.204\left(\frac{293}{T_m}\right),$$
$$\text{Pr} = \frac{\mu c_p}{k}.$$

Equations (1) to (26) constitute a nonlinear model for the solar air heater that has been used for the computation of the useful heat gain, thermal efficiency, and pumping power. The model has been solved by following an iterative process as depicted in Figure 3. For the heat collection estimate, the iteration was terminated when the successive values of the plate and mean air temperatures differed by less than 0.05 K. The iteration for the estimate of top loss has been continued till the heat loss estimates from the absorber plate to the glass cover and glass cover to the ambient; that is, Q_{tpg} and Q_{tgo} differed by less than 0.2%.

3. Experimental Setup

The experimental test facility, designed and fabricated as per ASHRAE Standard for testing of solar collectors [27], consists of 300 mm wide parallel ducts with entrance, test, exit, and mixing sections, a blower, control valves, orifice plates and provision for temperature, and pressure drop measurements as shown in Figure 4. It works in an open loop mode. The ducts are made of good quality smooth faced plywood and wooden boards. Each duct is 2880 mm long consisting of 550 mm long insulated entry and exit sections and 1.62 m long test section. The height of both the ducts has been kept fixed at 38.4 mm. The combined width of ducts (with side walls) is 850 mm.

The test section of one of the parallel ducts carries 3.25 mm thick aluminium plate in 12 equal width pieces as absorber plate with twelve aluminium sections 0.9 mm thick installed as baffles. Each baffle consists of one row of holes as shown in Figure 1(a). The other duct carries a three-piece smooth surfaced aluminium absorber plate. The sun-facing sides of both the absorber plates are smooth and blackened. Glass plates of 4 mm thickness have been used as cover over the absorber plates at a height of 60 mm. The top side of entry and exit lengths of each duct is covered with the plywood.

Table 1: Baffles and test duct details and experimental conditions.

Baffles (half-perforated baffles):
Baffle thickness, $\delta = 0.9$ mm
Height, $e = 19$ mm
Pitch, $p = 134.1$ mm
Relative baffle pitch, $p/e = 7.06$
Open area ratio, $\beta = 26\%$
Arrangement: transverse to the flow
Duct:
Width, $W = 298$ mm
Height, $H = 38.4$ mm
Length, $L = 1620$ mm
Hydraulic diameter, $D_h = 68$ mm
Baffle to duct height ratio, $e/H = 0.495$
Duct width to height ratio, $W/H = 7.77$
Collector aperture area, $A_a = 0.4 \times 1.62\ \text{m}^2$
Experimental conditions
Mass flow rate of air per unit area of the absorber plate, $G \approx 0.02$–$0.073\ \text{kgs}^{-1}\text{m}^{-2}$
Flow Reynolds number, Re $\approx$ 3000–11000
Solar insolation, $I = 585$–$710\ \text{Wm}^{-2}$
Wind velocity = 0.05–1.1 m s^{-1}

A 100 mm long baffled mixing section is provided to get uniform temperature of the exit air in the measuring section just after the mixing section. The exit end of each duct is connected, through a rectangular to circular transition piece, to a 68 mm ID G.I. pipe with orifice plate assembly. The throat diameter of the orifice plate is 38 mm. The other end of the each pipe is connected through control valve to the suction of a 10 HP blower using flexible pipe and a Y-section (not shown in the figure).

50 mm thick thermocole insulation has been provided on the back of the collector from test section inlet to outlet of twin duct, while the transition pieces and orifice plate assembly pipes (up to the orifice plates) are covered with foam blanket insulation. All joints are properly sealed with putty. The setup was installed horizontal (in north-south orientation) on the roof top at a height of 750 mm on an iron stand.

Butt-welded 0.36 mm calibrated copper-constantan thermocouples have been used for various temperature measurements. For the plate temperature measurement, thermocouples have been fixed with M-seal in the sun-facing side of absorber plate in small diameter holes drilled about 2.5 mm deep at nine and fourteen axial locations on the smooth and baffled absorber plates, respectively, as shown in Figure 4. Additional thermocouples have been affixed on the absorber plate of the baffled solar air heater to measure span wise variation of plate temperature. Three thermocouples are

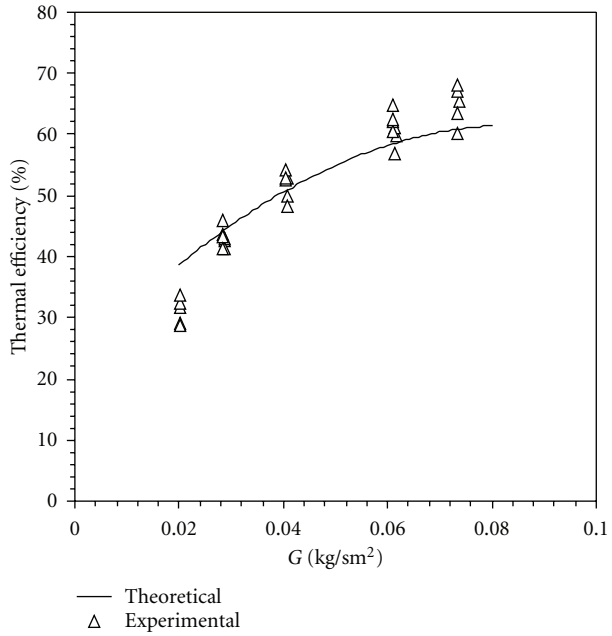

Figure 5: Thermal efficiency versus the flow rate per unit area of absorber plate for smooth duct air heater.

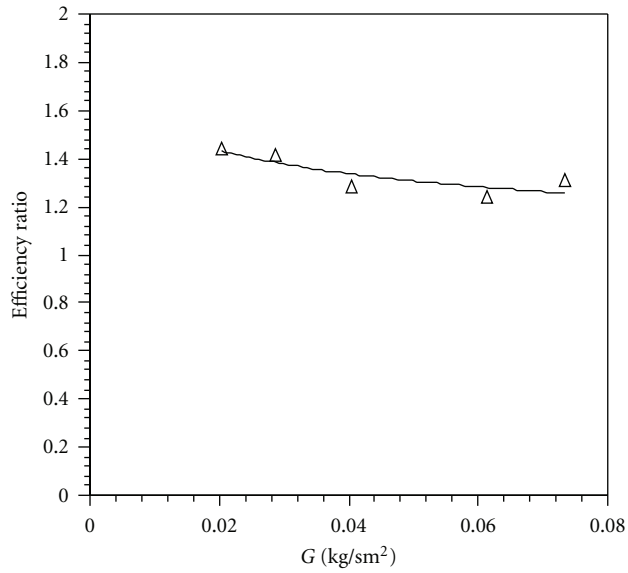

Figure 6: Efficiency ratio versus the flow rate per unit area of absorber plate.

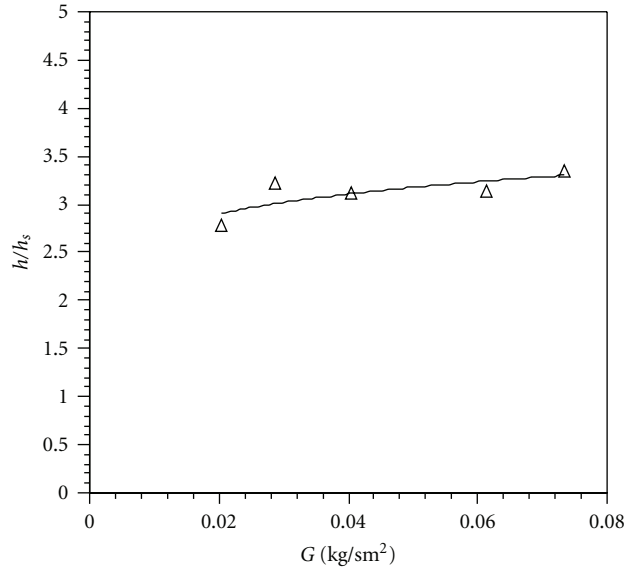

Figure 7: Heat transfer enhancement versus the flow rate per unit area of absorber plate.

placed in temperature measuring section after the mixing section to measure the outlet air temperature, while a thermocouple placed midway in the entry section measures the inlet air temperature.

Inclined U-tube manometers have been used for the measurement of pressure drop across the orifice plates. Pressure taps, located along the axial center line of the smooth lower wall of the both test sections, have been used to measure the static pressure drop across 1.62 m long test section using a null balance type micromanometer having a least count of 0.02 mm.

Calibrated precision solarimeter and pyranometer have been used for the measurement of the intensity of the solar radiation on the collector plane. The wind velocity has been measured by an anemometer.

The details of the half-perforated baffles employed in the study and other experimental conditions are given in Table 1. The baffles have one row of holes (3/8″ diameter) drilled in the lower half (near to the duct wall).

The open area ratio β of the perforated baffles is defined as the ratio of the area of the holes to the baffle frontal area given by

$$\beta = n\frac{(\pi/4)D^2}{be}, \tag{27}$$

where n is the number of the holes drilled, D is the diameter of a hole, e is the height and b is the width of the baffle.

Before starting the experiment, the setup and various components were checked for proper functioning. The glass covers were cleaned. Then, the blower was switched on, and the flow control valves were adjusted to give desired air flow rates through the ducts. All observations were made every 30 minutes starting from about 10 am till about 2 pm, that is, equally divided about the noon.

4. Data Reduction

The mass flow rate of air is determined from the measured pressure drop Δp_o across the orifice plate

$$m = c_d A_o \sqrt{\frac{2\Delta p_o p_a}{RT_o}}. \tag{28}$$

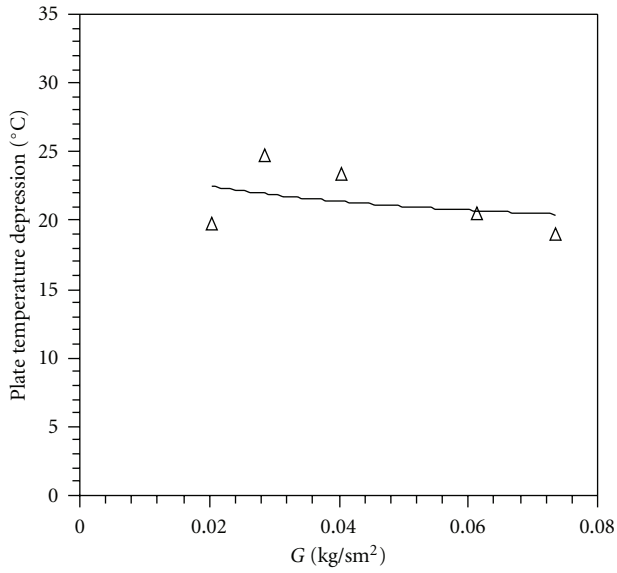

Figure 8: Absorber plate temperature depression.

Mass flow rate per unit area of the absorber plate G is calculated from

$$G = \frac{m}{A}, \tag{29}$$

where $A = WL$ is the absorber plate area.

The Reynolds number of the flowing air in the duct is calculated from

$$\mathrm{Re} = \frac{G_1 D_h}{\mu}, \tag{30}$$

where $G_1 = m/(WH)$ is mass velocity of air in the duct and $D_h = 4WH/[2(W + H)]$ is the hydraulic diameter of the duct.

Useful heat gain Q is the heat transferred to the air from the heated absorber plate and is obtained from

$$Q = mc_p(T_o - T_i). \tag{31}$$

Thermal efficiency η of the collector is ratio of useful heat gain to the incident solar radiation on the collector aperture area A_a

$$\eta = \frac{Q}{A_a I}. \tag{32}$$

The heat transfer coefficient has been calculated from

$$h = \frac{Q}{\left[A\left(T_p - T_m\right)\right]}, \tag{33}$$

where T_p is mean plate temperature calculated as the weighted average of temperature readings noted at various points along the axial length of the absorber plate; that is,

$$T_p = \left(\frac{1}{A}\right)\sum(T_i A_i). \tag{34}$$

In (33), T_m is the mean air temperature taken as arithmetic mean of the measured inlet and outlet air temperature values

$$T_m = \frac{T_i + T_o}{2}. \tag{35}$$

From the known values of pressure drop Δp_d across the test section and the mass flow rate, the pumping power is obtained from

$$P = \left(\frac{m}{\rho}\right)\Delta p_d\ . \tag{36}$$

From the analysis of uncertainties in the measurements by various instruments [28], the uncertainties (odds of 20 : 1) in the calculated values of various parameters have been estimated as follows:

flow rate per unit area of absorber plate, $G = \pm 1.6\%$,

heat collection rate, $Q = \pm 3.8\%$,

thermal efficiency, $\eta = \pm 4.9\%$,

pumping power, $P = \pm 4.3\%$.

5. Results and Discussion

The experimentally determined thermal efficiency data for the smooth duct solar air heater are plotted in Figure 5 against the flow rate per unit area of the absorber plate along with the predicted thermal efficiency from the mathematical model at the average values of the observed solar insolation, ambient temperature, and wind velocity during the experimentation. The absorber plate emissivity ε_p has been assumed to be 0.95, long wave emissivity of glass ε_g as 0.88, and transmittance-absorptance product $\tau\alpha$ as 0.8. The scatter in the experimental data is due to the variation in the ambient conditions. The theoretical analysis shows that the variation in the wind velocity has greater effect as compared to the variation in the ambient temperature and solar insolation in the experimental range of these parameters. At the lowest flow rate of the study, the experimental value of the thermal efficiency is lower due to a comparatively higher average wind velocity during experimentation at this flow rate, while the reverse is true at the highest flow rate of the study. Further, it is worth to note that, in general, the ambient temperature has been seen to rise with time (10 am to 2 pm) while the solar insolation increased up to the noon and then decreased. Thus, a transient condition exists, and the efficiency values in the morning and afternoon tend to lie below and above the mean values, respectively. Hence, looking to the effect of variation in the experimental conditions, the experimental and predicted values can be regarded to be in good agreement, and the presented model can be used to predict the performance of the solar air heater under a wide range of ambient (solar insolation, wind velocity, and ambient temperature) and air mass flow rate conditions.

For prediction of the performance of a roughened or baffled duct solar air heater, the Nusselt number and

Table 2: Values of different parameters for performance prediction of baffled duct solar air heater.

Collector width, W	1 m
Collector length, L	2 m
Duct height, H	35 mm
Gap between absorber plate and glass cover	50 mm
Collector slope, β	0° for horizontal
Number of glass covers	1
Transmittance-absorptance product, $\tau\alpha$	0.8 for single glass cover
Thickness of glass cover	4 mm
Thermal conductivity of glass cover	0.78 $Wm^{-1} K^{-1}$
Thermal conductivity of back insulation material (Thermocol)	0.037 $Wm^{-1} K^{-1}$
Back insulation thickness	50 mm
Long wave emissivity	0.88 for glass cover 0.95 for absorber with flat black paint
Relative baffle height, e/H	0.495
Relative baffle pitch, p/e	7.0
Sky temperature, T_s	$= T_a$
Ambient temperature, T_a	285–315 K
Wind heat transfer coefficient, h_w	5 and 10 $Wm^{-2} K^{-1}$
Solar insolation, I	500 and 800 Wm^{-2}

friction factor correlations of smooth duct air heater in the mathematical model are to be replaced by the appropriate correlations for the employed roughness or baffles.

It can be seen in Figure 5 that the thermal efficiency increases with increase in the flow rate, which is due to the increase in the heat transfer coefficient at the increased air velocity in the air heater duct.

Figure 6 shows the enhancement in the thermal efficiency due to the use of baffles on the air flow side of the absorber plate. The efficiency ratio in Figure 6 is the ratio of the thermal efficiencies of the baffled and smooth duct air heaters. The employment of the baffles enhances the thermal efficiency by about 28%–45%; higher gain is at the lowest air flow rate of the study. The thermal performance advantage of the baffled duct solar air heater can be attributed to the heat transfer enhancement (h/h_s, where h_s refers to the smooth duct) of about 180%–235% as depicted in Figure 7. The effect of the perforated baffles on the flow structure and resulting heat transfer enhancement has been discussed earlier.

The increase in the heat transfer coefficient due to the baffles also reduces the mean absorber plate temperature of the baffled absorber plate by about 20°C–25°C as compared to the smooth duct air heater absorber plate; see Figure 8. This leads to a reduction in the heat loss from the collector, which is a function of the excess of the absorber plate temperature over the ambient temperature. The increase in the heat collection rate due to the heat transfer enhancement and decrease in the heat loss from the collector due to the lower working temperature of the absorber plate enhance the thermal efficiency of the baffled air heater.

The pumping power requirement has been found to be negligible (less than 0.5% of the heat collection rate). Thus, thermohydraulically, the baffled duct solar air heater is better than the smooth duct solar air heater.

6. Performance Prediction of Baffled Duct Air Heater

For half-perforated baffles in an asymmetric heated rectangular duct, Karwa and Maheshwari [18] have presented the following correlations of Nusselt number and friction factor:

$$\begin{aligned} \mathrm{Nu} &= 0.0893\mathrm{Re}^{0.7608}, \\ f &= 0.1673\mathrm{Re}^{-0.0213}, \end{aligned} \tag{37}$$

with standard deviation of 1.34% and 3.34%, respectively, from the experimental data.

Using the mathematical model presented above, performance study of baffled duct solar air heater has been carried out by replacing the Nusselt number and friction factor correlations for the smooth duct in the mathematical model by the above correlations for the baffled duct solar air heater. Table 2 gives values of different parameters used in the study.

In Figure 9, the plots of thermal efficiency and effective efficiency of the baffled duct solar air heater are presented against the temperature rise parameter $\Delta T/I$ for fixed geometric and ambient parameters. Their values are also given in a tabular form. The effective thermal efficiency takes account of pumping power and is defined as [19]

$$\eta_{\mathrm{eff}} = \frac{(Q + P - P/C)}{IA}. \tag{38}$$

In the above equation, factor C is a conversion factor for calculating equivalent thermal energy for the pumping power. It is a product of efficiency of fan, motor, transmission and that of thermoelectric conversion at the power plant. For a fan-motor efficiency of 0.6 and thermoelectric conversion efficiency referred to the consumer point as 0.33, the factor C works out to be 0.2. It is to note that pumping power P required to overcome friction is also converted into heat.

It can be seen in Figure 9 that the pumping power is not of a concern at low flow rates. At the highest flow rate of the study ($G = 0.07\,\mathrm{kg/sm^2}$), the effective efficiency is about 5% lower than the thermal efficiency as also given in the table.

The plot in Figure 9 can be utilized for performance prediction of such air heater. The use of the plot is simple. For example, let for a given application the required air temperature rise is 12°C when solar insolation is 800 W/m^2. Then, the temperature rise parameter $\Delta T/I$ works out to be 0.015. A vertical line on the plot in Figure 9 at $\Delta T/I = 0.015$ gives thermal efficiency η of about 67.5%. Using the basic

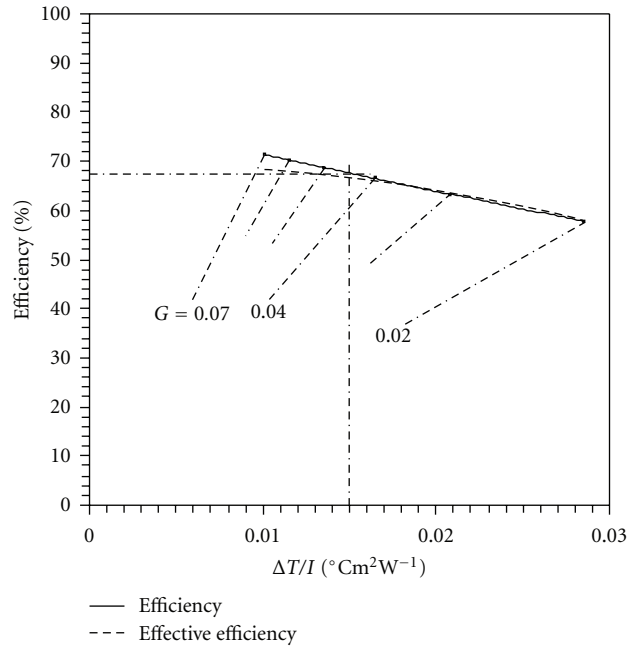

G, kg/sm^2	0.02	0.03	0.04	0.05	0.06	0.07
Thermal efficiency, η (%)	57.73	63.22	66.45	68.62	70.13	71.23
Effective efficiency, η_{eff}(%)	57.64	62.94	65.81	67.37	68.0	67.87

Figure 9: Thermal efficiency and effective efficiency as function of temperature rise parameter ($W = 1$ m, $L = 2$ m, $H = 0.035$ m, $I = 800$ W/m^2, slope $= 0$ deg; $h_w = 5$ W/m^{2}K, $T_a = 300$ K, and $G = 0.02$–0.07 kg/sm^2).

equation of thermal efficiency, the air mass flow rate per unit area of the absorber plate is estimated as

$$G = \frac{(\eta I)}{\left[c_p \Delta T\right]} = \frac{(0.675 \times 800)}{(1005 \times 12)} = 0.045\,\text{kg/sm}^2. \quad (39)$$

7. Effect of Variation of Ambient Parameters on Thermal Efficiency

The performance plot in Figure 9 has been presented for fixed values of solar insolation, wind velocity, and ambient temperature. These parameters, especially the solar insolation and ambient temperature, vary from morning to evening (9 AM to 4 PM) and also with the season of the year. The effect of their variation on the thermal efficiency of the baffled duct solar air heater is presented in Figures 10, 11, and 12

From Figures 10–12, it can be seen that effect of variation of the solar insolation from $I = 800$ W/m^{2}sto 500 W/m^2 is not significant, while the increase in wind heat transfer coefficient from 5 W/m^{2}K to 10 W/m^{2}K reduces the thermal efficiency at the lowest flow rate by about 4%, which can be termed as significant. At the highest flow rate of the study (the lowest temperature rise parameter and extreme left end of these curves), the thermal efficiency is less affected by variation of these parameters. The thermal performance of the air heater improves by about 1.8% in the winter ($T_a = 285$ K) and reduces by about 2% in summer ($T_a = 315$ K) at the lowest flow rate. At low ambient temperature and solar insolation, the operating temperature of the collector reduces and thermal efficiency improves, while a high wind velocity increases the heat loss from the collector.

The results of the present study can be utilized for the development of enhanced performance solar air heater with half-perforated baffles.

8. Conclusions

An experimental study on thermal performance of a solar air heater having half-perforated baffles on the air flow side of the absorber plate has been carried out for air mass flow rate of about 0.02–0.073 kg/s per m^2 of the absorber plate area. A direct comparison of performance with the smooth duct solar air heater has been made, and a detailed mathematical model has been presented. The main findings of the present study are as follows.

(1) The predicted values of thermal efficiency from the mathematical model for the smooth duct solar air heater are in good agreement with the experimental data. Hence, the model can be used for performance prediction under wide range of operating and ambient conditions.

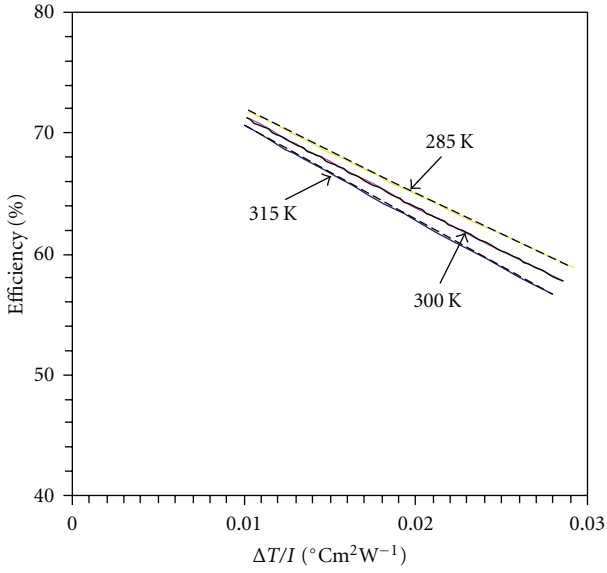

Figure 10: Effect of ambient temperature ($W = 1$ m, $L = 2$ m, $H = 0.035$ m, slope = 0 deg; $I = 800$ W/m2, $h_w = 5$ W/m^{2}K).

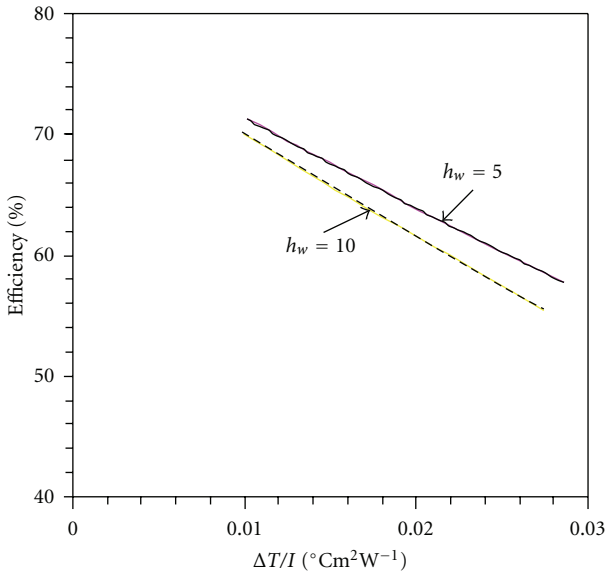

Figure 11: Effect of wind heat transfer coefficient ($W = 1$ m, $L = 2$ m, $H = 0.035$ m, slope = 0 deg; $I = 800$ W/m^2, $T_a = 300$ K).

(2) The thermal efficiency of the baffled duct solar air heater is about 28%–45% higher than the smooth duct solar air heater; highest thermal performance advantage is at the lowest flow rate of the study.

(3) The heat transfer enhancement due to the baffles (of the order of 180%–235%) increases the heat collection rate and reduces the mean temperature of the baffled absorber plate by 20°C–25°C as compared to the smooth one.

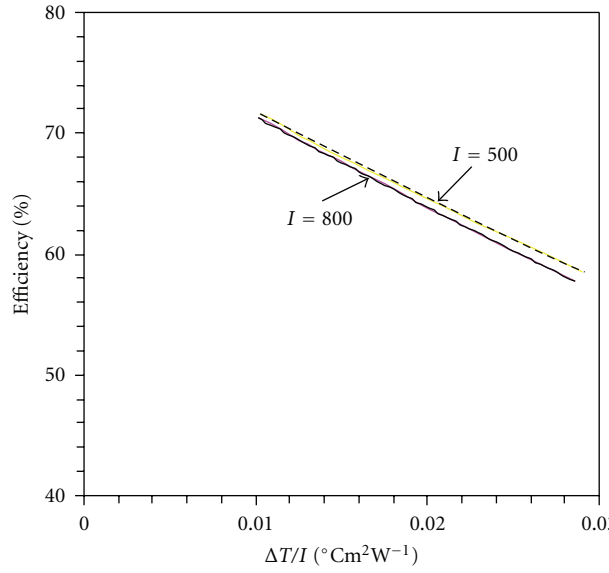

Figure 12: Effect of solar insolation ($W = 1$ m, $L = 2$ m, $H = 0.035$ m, slope = 0 deg; $h_w = 5$ W/m^{2}K, $T_a = 300$ K).

(4) The pumping power requirement is only a small fraction of the heat collection rate in the range of the present study.

(5) Effect of variation of solar insolation on the thermal performance is negligible (0.4%–1.42%), while the variation in wind heat transfer coefficient affects the efficiency by 1.6%–4.3% and the ambient temperature by (±0.8%) to (±2.0%); the higher values in all cases refer to the lowest flow rate of the study.

Nomenclature

A: Absorber plate area = WL, m^2
A_a: Collector aperture area, m^2
A_o: Orifice throat area, m^2
D_h: Hydraulic diameter of duct = $4WH/[2(W + H)]$, m
e: Height of baffle, mm
c_d: Coefficient of discharge
c_p: Specific heat, Jkg^{-1}K^{-1}
f: Fanning friction factor
g: Acceleration due to gravity, ms^{-2}
G: Mass flow rate per unit area of plate = m/A, kg s^{-1} m^{-2}
G_1: Mass velocity = $m/(WH)$, kg s^{-1} m^{-2}
H: Air flow duct height (depth), m
h_w: Wind heat transfer coefficient, Wm^{-2}K^{-1}
I: Solar radiation on the collector plane, Wm^{-2}
k: Thermal conductivity of air, Wm^{-1}K^{-1}
L: Length of collector, length of test section, m
m: Mass flow rate, kgs^{-1}
Nu: Nusselt number

p: Baffle pitch, m
P: Pumping power, W
Pr: Prandtl number = $\mu c_p/k$
p_a: Ambient pressure, Nm^{-2}
Δp_d: Pressure drop across duct, Nm^{-2}
Δp_o: Pressure drop across orifice plate, Nm^{-2}
p/e: Relative baffle pitch
Q: Useful heat gain, W
R: Gas constant, $Jkg^{-1}\,K^{-1}$
Re: Reynolds number = $G_1 D_h/\mu$
T_a: Ambient temperature, K
T_{fm}, T_m: Mean air temperature = $(T_o + T_i)/2$, K
T_i: Inlet air temperature, K
T_{mpg}: Mean of the plate and glass temperatures = $(T_p + T_{gi})/2$, K
T_o: Outlet air temperature, K
T_p: Mean plate temperature, K
T_s: Sky temperature, K
U_L: Overall loss coefficient, $Wm^{-2}K^{-1}$
W: Width of the duct, m.

Greek Symbols

β: Collector slope, deg
δ_{pg}: Gap between the absorber plate and glass cover, m
ΔT: Air temperature rise = $T_o - T_i$, K
$\Delta\eta$: Change in thermal efficiency
ε: Emissivity
η: Thermal efficiency = $Q/(IA)$
η_e: Effective efficiency,(38)
μ: Dynamic viscosity, Pa s
ν_{mpg}: Kinematic viscosity of air at temperature T_{mpg}, m^2s^{-1}
ρ: Density of air, kg m^{-3}
$\tau\alpha$: Transmittance-absorptance product.

Subscripts

b: Duct bottom surface
g: Glass
m: Mean
p: Plate.

References

[1] D. Gupta, S. C. Solanki, and J. S. Saini, "Thermohydraueic performance of solar air heaters with roughened absorber plates," *Solar Energy*, vol. 61, no. 1, pp. 33–42, 1997.

[2] R. Karwa, S. C. Solanki, and J. S. Saini, "Thermo-hydraulic performance of solar air heaters having integral chamfered rib roughness on absorber plates," *Energy*, vol. 26, no. 2, pp. 161–176, 2001.

[3] M. M. Sahu and J. L. Bhagoria, "Augmentation of heat transfer coefficient by using 90° broken transverse ribs on absorber plate of solar air heater," *Renewable Energy*, vol. 30, no. 13, pp. 2057–2073, 2005.

[4] A. R. Jaurker, J. S. Saini, and B. K. Gandhi, "Heat transfer and friction characteristics of rectangular solar air heater duct using rib-grooved artificial roughness," *Solar Energy*, vol. 80, no. 8, pp. 895–907, 2006.

[5] A. Layek, J. S. Saini, and S. C. Solanki, "Second law optimization of a solar air heater having chamfered rib-groove roughness on absorber plate," *Renewable Energy*, vol. 32, no. 12, pp. 1967–1980, 2007.

[6] M. K. Mittal, Varun, R. P. Saini, and S. K. Singal, "Effective efficiency of solar air heaters having different types of roughness elements on the absorber plate," *Energy*, vol. 32, no. 5, pp. 739–745, 2007.

[7] M. K. Gupta and S. C. Kaushik, "Performance evaluation of solar air heater for various artificial roughness geometries based on energy, effective and exergy efficiencies," *Renewable Energy*, vol. 34, no. 3, pp. 465–476, 2009.

[8] R. Karwa, N. Karwa, R. Misra, and P. C. Agarwal, "Effect of flow maldistribution on thermal performance of a solar air heater array with subcollectors in parallel," *Energy*, vol. 32, no. 7, pp. 1260–1270, 2007.

[9] S. Singh, S. Chander, and J. S. Saini, "Thermal and effective efficiency based analysis of discrete V-down rib-roughened solar air heaters," *Journal of Renewable and Sustainable Energy*, vol. 3, no. 2, Article ID 023107, 2011.

[10] A. Lanjewar, J. L. Bhagoria, and R. M. Sarviya, "Experimental study of augmented heat transfer and friction in solar air heater with different orientations of W-Rib roughness," *Experimental Thermal and Fluid Science*, vol. 35, no. 6, pp. 986–995, 2011.

[11] R. Karwa, "Experimental studies of augmented heat transfer and friction in asymmetrically heated rectabgular ducts with ribs on the heated wall in transverse, inclined, v-continous and v-discrete pattern," *International Communications in Heat and Mass Transfer*, vol. 30, no. 2, pp. 241–250, 2003.

[12] J. J. Hwang, T. Y. Lia, and T. M. Liou, "Effect of fence thickness on pressure drop and heat transfer in a perforated-fenced channel," *International Journal of Heat and Mass Transfer*, vol. 41, no. 4-5, pp. 811–816, 1998.

[13] J. J. Hwang and T. M. Liou, "Augmented heat transfer in a rectangular channel with permeable ribs mounted on the wall," *Journal of Heat Transfer*, vol. 116, no. 4, pp. 912–920, 1994.

[14] J. J. Hwang and T. M. Liou, "Heat transfer in a rectangular channel with perforated turbulence promoters using holographic interferometry measurement," *International Journal of Heat and Mass Transfer*, vol. 38, no. 17, pp. 3197–3207, 1995.

[15] T. M. Liou and S. H. Chen, "Turbulent heat and fluid flow in a passage disturbed by detached perforated ribs of different heights," *International Journal of Heat and Mass Transfer*, vol. 41, no. 12, pp. 1795–1806, 1998.

[16] O. N. Sara, T. Pekdemir, S. Yapici, and M. Yilmaz, "Heat-transfer enhancement in a channel flow with perforated rectangular blocks," *International Journal of Heat and Fluid Flow*, vol. 22, no. 5, pp. 509–518, 2001.

[17] R. Karwa, B. K. Maheshwari, and N. Karwa, "Experimental study of heat transfer enhancement in an asymmetrically heated rectangular duct with perforated baffles," *International Communications in Heat and Mass Transfer*, vol. 32, no. 1-2, pp. 275–284, 2005.

[18] R. Karwa and B. K. Maheshwari, "Heat transfer and friction in an asymmetrically heated rectangular duct with half and fully perforated baffles at different pitches," *International Communications in Heat and Mass Transfer*, vol. 36, no. 3, pp. 264–268, 2009.

[19] R. Karwa and K. Chauhan, "Performance evaluation of solar air heaters having v-down discrete rib roughness on the absorber plate," *Energy*, vol. 35, no. 1, pp. 398–409, 2010.
[20] S. A. Klein, "Calculation of flat-plate collector loss coefficients," *Solar Energy*, vol. 17, no. 1, pp. 79–80, 1975.
[21] H. Buchberg, I. Catton, and D. K. Edwards, "Natural convection in enclosed spaces—a review of application to solar energy collection," *Journal of Heat Transfer*, vol. 98, no. 2, pp. 182–188, 1976.
[22] P. W. Niles, E. J. Carnegie, J. G. Pohl, and J. M. Cherne, "Design and performance of an air collector for industrial crop dehydration," *Solar Energy*, vol. 20, no. 1, pp. 19–23, 1978.
[23] M. A. Ebadian and Z. F. Dong, "Forced convection, internal flow in ducts," in *Handbook of Heat Transfer*, W. M. Rohsenow, J. P. Hartnett, and Y. I. Cho, Eds., chapter 5, McGraw-Hill, New York, NY, USA, 1998.
[24] K. G. T. Hollands and E. C. Shewen, "Optimization of flow passage geometry for air-heating, plate-type solar collectors," *Journal of Solar Energy Engineering, Transactions of the ASME*, vol. 103, no. 4, pp. 323–330, 1981.
[25] M. S. Bhatti and R. K. Shah, "Turbulent and transition flow convective heat transfer," in *Handbook of Single-Phase Convective Heat Transfer*, S. Kakac, R. K. Shah, and W. Aung, Eds., chapter 4, Wiley, New York, NY, USA, 1987.
[26] J. P. Holman, *Heat Transfer*, McGraw-Hill book Co., New York, NY, USA, 7th edition, 1990.
[27] ASHRAE Standard 93-77, "Methods of testing to determine the thermal performance of solar collectors," Tech. Rep., American Society of Heating, Refrigerating and Air-Conditioning Engineers, Inc., New York, NY, USA, 1977.
[28] S. J. Kline and F. A. McClintock, "Describing uncertainties in single sample experiments," *Mechanical Engineering*, vol. 75, pp. 3–8, 1953.